Impact of the Zn source on the RSN-type zeolite formation

Ana Palčić, Bartlomiej M Szyja, Maja Mičetić, Tomaž Čendak, Mariame Akouche, Krunoslav Juraić, Marija Čargonja, Darko Mekterović, Vitomir Vušak, Valentin Valtchev

Impact of Zn source on the RSN-type zeolite formation

Ana Palčić[a*], Bartłomiej M. Szyja[b], Maja Mičetić[c], Tomaž Čendak[d], Mariame Akouche[e], Krunoslav Juraić[c], Marija Čargonja[f], Darko Mekterović[f], Vitomir Vušak[g] and Valentin Valtchev[e]

[a] Division of Materials Chemistry, Ruđer Bošković Institute, Bijenička 54, 10000 Zagreb, Croatia.
[b] Faculty of Chemistry, Wrocław University of Science and Technology, Gdańska 7/9, 50-344 Wrocław, Poland.
[c] Division of Materials Physics, Ruđer Bošković Institute, Bijenička 54, 10000 Zagreb, Croatia.
[d] Department of Inorganic Chemistry and Technology, National Institute of Chemistry, Hajdrihova 19, SI-1001 Ljubljana, Slovenia.
[e] Normandie Univ, ENSICAEN, UNICAEN, CNRS, Laboratoire Catalyse et Spectrochimie, 6 Marechal Juin, 14050 Caen, France
[f] University of Rijeka, Department of Physics, Ulica Radmile Matejčić 2, 51000 Rijeka, Croatia
[g] Pliva Croatia Ltd., Prilaz baruna Filipovića 25, 10000 Zagreb, Croatia.

*e-mail: ana.palcic@irb.hr

Abstract

Typical zeolite synthesis reaction mixture involves framework atom source, solvent, mineraliser, and structure directing agent. However, these components often have a dual function, and their impact on the nucleation/crystallization process is difficult to be established straightforwardly. The present study deals with the structure directing effect of zinc in the preparation of zincosilicate RUB-17 (RSN-type material). First, an attempt was made to introduce several other heteroatoms (Al, B, Ge, Mg, Li, Zr) into the RSN framework under the same reaction conditions as for Zn-RSN. Second, different Zn sources have been employed in order to study their impact on RUB-17 intermediates and the final product properties. The obtained series of samples were analysed by XRD, XRF, GISAXS, SEM, TEM, TG as well as by Raman, NMR, infrared and solid state UV/VIS spectroscopy. The physicochemical analysis of the obtained solids were complemented by the DFT modelling. The results show that RSN-type material can be solely prepared in the Zn-containing systems, where zinc plays a structure directing role besides its function as a framework cation. Namely, the *lov*-unit, a basic building unit of RSN framework, is formed at the very beginning of the crystallization no matter the zinc source employed. Yet, the differences in the crystallization of different system and relatively long time needed for full transformation of the precursor indicates there is some other limiting step that accounts for the formation of the zeolite.

Keywords: zeolite synthesis, zinc, silicate, three-membered ring, structure directing, precursor

Introduction

According to the classical definition, zeolites are crystalline tectosilicates with a well-defined system of channels and cages with size below 2 nm. The pore size categorizes zeolites as microporous materials by IUPAC classification. Nowadays this definition is extended to all materials possessing structure features typical for zeolites: tetrahedra of oxygen atoms bonded to central T atom (T = Si, Al, P, Ge, Zn, Ga, …) connected via vertices thus forming 3D porous framework.[1] Zeolites are widely used materials in various areas of human activities. The most common and the largest volume of application involves their usage as catalysts, ion exchangers, sorbents and separation materials.[2-6] The extensive and continuously expanding range of zeolites usage is a direct consequence of their tuneable set of properties ensuing from their unique chemical composition and framework structure. For example, introducing T-atoms other than silicon and aluminium (heteroatoms) in the zeolite framework can result in different properties of the materials in terms of hydrophobicity, acidity, ion-exchange capacity, and hydrothermal stability.[7] Typical examples are Al-MFI (ZSM-5), Si-MFI (silicalite-1) and Ti-MFI (TS-1) materials. ZSM-5 is a good acid catalyst (xylene isomerization, FCC, MTG, etc.), whereas TS-1 is active in oxidation reactions (epoxidation of alkenes, cyclohexanone ammoxidation, etc.).[8,9] In addition, some of the zeolite frameworks have been prepared solely in the presence of a particular heteroatom such as ECR-34 and VPI-9 containing gallium and zinc, respecitvely.[7]

In order to enhance the efficacy and activity of zeolite materials, further studies should be conducted. Preparation and detailed characterization of new materials and improving the properties of "classical" zeolites (materials of desired size, morphology, acidity, ion-exchange capacity, hierarchization,…) are the two principal axes of research in zeolite science.[10-16] Understanding the mechanisms of formation of a particular material could enable the preparation of materials having the same structure but variable chemical composition and consequently different properties. Herein, the zincosilicate material RUB-17, which is so far the only known RSN-type zeolite material, is investigated.[17] Its structure is built of 3-, 4-, 5-, and 6-membered rings forming a tridimensional system of channels 9(3.3×4.4Å) × 9(3.1×4.3Å) × 8(3.4×4.1Å). 3MR frameworks are of particular importance since it has been theoretically predicted that the structures composed of small rings (3MRs and 4MRs) should exhibit lower framework density.[7] More open microporous frameworks offer new possibilities to overcome diffusion limitations and process bulkier molecules. Moreover, the 9-membered ring containing materials are expected to have interesting performance in separation processes.

It should be stressed that in total there are 24 3MR containing zeolitic framework types, many of them having only one representative type material. Some of them are not silicates (e.g. gallogermanates) and still there is only one known 3MRs alumosilicate zeolite material (MEI-type).[18] Further, heteroatoms such as Be, Zn, Li and Ge were incorporated in the 3MRs silicate materials (OSB-1, VPI-9, RUB-29, ITQ-40), where Be and Zn are present in many zeolitic materials, particularly natural zeolites (LOV-, NAB- and VSV-type materials). In addition, most of Be and Zn zeolites are built of *lov*-unit which comprises two 3MRs sharing one vertex (spiro center).[18] For this study zincosilicate zeolitic material RUB-17 was chosen due to the availability and non-toxicity of zinc. The results of the investigation of the impact of the employed zinc source on the formation of RUB-17 material and its properties are presented. The data will provide new findings on the processes affecting the synthesis of the 3MR-

containing zincosilicate materials and represent a basis for the design of zeolite materials with novel functions.

Experimental part

Synthesis of materials containing various T atoms. In order to study the impact of the presence of T atoms other than zinc, reaction mixtures have been prepared in a procedure analogous to the one reported in reference[17]. The molar oxide composition of the studied reaction mixtures was 1 SiO_2 : 0.1 TO : 0.5 NaOH : 0.5 KOH : 0.08 TEAOH : 44 H_2O. The framework T atom sources were as follows: aluminium (Al powder, puriss., Kemika) aluminium hydroxide ($Al(OH)_3$, w(Al_2O_3) = 63-67%, Riedel de Haën), sodium aluminate ($NaAlO_2$, w(Al_2O_3) = 54%, Riedel de Haën), germanium oxide (GeO_2, 99.99%, Sigma Aldrich), lithium hydroxide monohydrate ($LiOH \cdot H_2O$, 99%, Sigma Ultra), boric acid ($B(OH)_3$, p.a., Kemika), boron oxide (B_2O_3, 99.99%, Ventron), zirconyl chloride octahydrate ($ZrOCl_2 \cdot 8H_2O$, 98%, Aldrich), zirconium(IV) isopropoxide ($Zr(OCH(CH_3)_4 \cdot (CH_3)_2CHOH$, 99.9%, Aldrich) and magnesium oxide (MgO, 99.99%, Merck). The reactions have been conducted at 180 °C from 11 to 60 days (Table 1). The solids have been recovered by filtration and repeatedly washed until the pH value of the supernatant had reached 7.

RUB-17 synthesis. Zincosilicate RUB-17 was prepared as previously described.[17] Needed amounts of sodium hydroxide (pellets, 97%, Acros organics), potassium hydroxide (pellets, 85%, Kemika), tetraethylammonium hydroxide (TEAOH, 35% water solution, Aldrich), a zinc source, and doubly distilled water were mixed. The employed zinc sources were zinc oxide (ZnO, 99.9%, Ventron), zinc chloride ($ZnCl_2$, 98%, Sigma), zinc bromide ($ZnBr_2$, purum p.a., Fluka), zinc nitrate hexahydrate ($Zn(NO_3)_2 \cdot 6H_2O$, p.a., Kemika), zinc acetate dihydrate ($Zn(OAc)_2 \cdot 2H_2O$, p.a., Kemika), zinc acetylacetonate monohydrate ($Zn(acac)_2 \cdot H_2O$, prepared according to the previously published procedure[19]) and zeolitic imidazolate framework material number 8 (ZIF-8, prepared according to the previously published procedure[20]). Upon treatment in an ultrasonic bath for 30 minutes, tetraethoxysilane (TEOS, 98 %, Aldrich) was added to the reaction mixture and hydrolyzed for 8 h at room temperature. The final molar oxide composition of the starting reaction system was 1 SiO_2 : 0.1 ZnO : 0.5 NaOH : 0.5 KOH : 0.08 TEAOH : 44 H_2O. The reaction mixture was transferred into Teflon lined autoclave and subjected to hydrothermal treatment at 180 °C for 11 days. The final product was recovered by filtration and repeatedly washed until the pH value of the supernatant had reached 7.

Characterization of the materials. The phase composition of the prepared solid materials was identified by X-ray diffraction (XRD) analysis of the powder samples collected by a PHILIPS PW 1840 X-ray diffractometer (Philips Analytical B. V., Almelo, The Netherlands) with $CuK_{\alpha 1}$ (λ = 1.54056 Å) radiation at 40 mA and 40 kV. The scattered intensities were measured with a scintillation counter. The samples were scanned in the range of Bragg angles 2θ = 5–50°. SEM micrographs were acquired by high resolution scanning electron microscope JEOL JSM-7000F. For transmission electron microscopy imaging a small amount of the sample was dispersed in ethanol. After being treated by ultrasonication, one drop of the sample mixture was taken from the ethanol solution and transferred to a copper grid covered by a holey carbon film. Transmission electron microscope JEOL JEM-3010 was used for TEM studies. A Gatan 794 CCD camera was used for recording transmission electron microscopy images.

Thermogravimetric analysis of the solid samples was performed with a Setaram Setsys TGA instrument. The heating rate was 5 °C min^{-1} and the samples were heated up to 800 °C in air flow. FT-IR spectra of the solid samples were recorded on a Bruker TENSOR 37 spectrometer using KBr pellets, in the range from 400 to 4000 cm^{-1}. Raman spectra were acquired by employing PD-LD LS2 laser source (784.2 nm, 450 mW) with optical fibers. The Raman probe (BWTEK) was coupled with Maya 2000 Pro spectrometer (Oceanoptics). Shimadzu UV-3600 UV/Vis/NIR spectrometer was used to obtain solid state UV-Vis spectra of the studied samples mixed with $BaSO_4$ powder supplied by Wako Pure Chemical Industries Ltd. The weight percentage of the samples was 1-5 wt%. The spectra were recorded at 20 °C in the range from 1200 to 200 nm at a resolution of 1 nm. The instrument was linked to an integrating sphere. The background was recorded using pure $BaSO_4$.

Zn/Si ratio of the solid samples was determined by employing Energy Dispersive X-Ray Fluorescence (ED-XRF) spectrometer. Powder samples were pressed into pellets with a 7 mm diameter and attached to a carbon tape prior to analysis. Rhodium X-ray tube (X-Ray Optical Systems, model X-Beam) was used for ionisation under 50 kV and 0.04 mA. Each sample was irradiated for 30 min with a beam collimated to a diameter of 2 mm and perpendicular to the sample. Characteristic X-rays were collected with silicon-drift detector (Amptek X-123SDD, resolution of 145 eV for Fe-Kα line) positioned at 45° with respect to the incoming beam. The measurements were performed in air, with 10 mm of source to sample distance and 25 mm of target to detector distance. The resulting X-ray spectra were fitted using the Quantitative X-ray Analysis System (QXAS) software developed by the International Atomic Energy Agency (IAEA) in order to obtain characteristic line intensities.[21] The Si/Zn ratios were calculated from the ratio of these intensities. The detailed description of the calculation procedure is presented in the Supporting information.

^{1}H–^{29}Si CPMAS NMR spectra were recorded on a 600 MHz Varian NMR System equipped with a 3.2 mm Varian MAS probehead. Larmor frequency for ^{29}Si nuclei was 119.088 MHz. Chemical shifts of the ^{29}Si nuclei are reported relative to the signal of ^{29}Si in tetramethylsilane. All measurements were executed at sample rotation frequency of 20 kHz, with relaxation delay of 2 s and CP contact time of 5 s. For the crystalline RUB-17 samples prepared using ZIF-8 and $Zn(NO_3)_2 \cdot 6H_2O$ as zinc source chemicals 10000 scans were accumulated with acquisition time of 40 ms and 80 kHz XiX decoupling. For the rest of the samples, 28000 scans were accumulated with acquisition time of 15 ms and 90 kHz XiX decoupling.

Structural properties of the materials including the size and arrangement of nanovoids were analysed by grazing incidence small angle X-ray scattering (GISAXS). GISAXS measurements were carried out at Elettra synchrotron Trieste (SAXS beamline), using X-ray beam with an energy of 8 keV and 2D Dectris photon detector (Pilatus 1M). The measured data were simulated and analysed using GisaxStudio software.[22,23] The powder materials were pressed into a thin tile before the GISAXS measurements.

Model and computational details. All simulations have been carried out using the DFT methodology. The generalized gradient approximation of PBE functional form[24] has been used, as implemented in the CP2k code.[25] In this approach mixture of the localized atomic orbitals (SZV molopt basis set) to represent the wavefunctions and the plane wave basis set (450 eV cutoff energy) to represent the electronic density.[26] The initial models have been optimized to reach forces lower than 0.5 eV/A. For each of the investigated models, the molecular dynamics

simulation has been carried out in NVT ensemble. The temperature was set to 298 K and controlled by Nose thermostat.[27] The timestep was set to 0.5 fs and total simulation time to 25 ps (50000 steps). The occurrence of the reaction was ensured by the gradual change of the distance between the oxygen of the water molecule and one of the T-atoms of interest (Si, Al or Zn). The initial distance was the result of the optimization of the geometry of the system, and the final distance was the average distance between the T-atom and oxygen in the structure (~1.60 A). The charge of the system has been set accordingly (0, -1 and -2 for Si, Al and Zn respectively).

In order to obtain a meaningful result, several parallel runs need to be executed to account for random initial velocities. For the needs of this work 20 runs have been carried out for each system, however due to the small differences in the models and similar constraints imposed - all runs have been observed to occur identically, and they led to the same results. The structure representing a computational model has been cut out from the crystal structure recovered from a .cif file available at International Zeolite Association website.[18] It consists of a 3-member ring, with none (pure silica) or one heteroatom (Al, Zn) present. It is basically the half of the symmetric *lov*-unit. The position of the heteroatom is in the vertices of the *lov*-unit, not in the spiro position. The building unit was embedded in the framework represented by 4 other T sites. In order to maintain the geometry of the cluster constructed this way, the Si atoms of the framework have been saturated with hydrides, and the positions of these hydrides were kept frozen during the simulations. The model is shown in Figure S1. Si atoms are represented by yellow spheres, O – smaller red spheres, H – smallest white spheres. Heteroatom is represented by a pink sphere.

The model represents the fully formed building unit, at the end of the process. In other words, the reaction that is carried out in this computational work is reversed and simulates the decomposition of the ring. This approach allows for better control of the process because it always leads to the desired product, i.e. the initial geometry in the MD simulation. At the same time, the transition state structures are the same as if the process was reversed, thus allowing to estimate the energetics of the reaction. This is “de facto” a kinetic approach - under the assumption that the thermodynamics of the process is always the same because from the same reactants (open ring) the same products (closed ring + water) are obtained. The thermodynamic stability of different structures (pure silica and two with heteroatoms) cannot be compared directly because of different composition of those systems, but for each process, ΔH can be calculated and compared with other systems. For each of the systems – pure silica, Al heteroatom, and Zn heteroatom, two kinds of simulations were carried out. One with the water cleaving a bond between the heteroatom or Si atom in the same position or the Si atom in the top vertex of the 3-ring. This approach allowed to identify whether one of these bonds has a different activation barrier - thus whether it is easier to cleave. This approach also allows to asses if the heteroatom is built in a vacancy (“nest”) already formed by Si sites, or actively drives the process towards this particular structure.

Results and discussion

Effect of T atoms

Several different T atoms (Al, B, Ge, Mg, Li, Zr) and all-silica RSN-type material have been attempted to crystallize. These heteroatoms were selected because they were found to form

three-membered ring units in various silicate systems, not always in zeolitic structures. Aluminium is the most common T atom after Si in zeolites and is present in the only 3MRs containing alumosilicate ZSM-18.[18] Germanium, and boron are incorporated into three-membered rings within zeolite-type frameworks while lithium and zirconium are present in three-membered ring silicate materials,[18,28,29] and magnesium favours the formation of 3MRs in silica glasses.[30] The molar oxide composition of the starting reaction mixtures and the chemicals used are similar with those employed in the RUB-17 preparation.[17] The chemicals employed as the sources of T atoms, the crystallization periods (t_C) and the final products are listed in the Table 1. Representative X-ray powder diffraction patterns of the obtained solids are displayed in Figure S2. The collected data show that RSN-type material was not obtained in any of the investigated systems. No solid product was found in the all-silica as well as in Li-containing system even after 60 days heating period. Magnesium-containing system yielded a layered-type material. In boron system the precipitation depends on the starting chemical. When boron hydroxide is employed highly crystalline phyllosilicate material is obtained, in contrast to the boron oxide system where no solid material was found. The use of two different zirconium sources, zirconyl chloride octahydrate and zirconium(IV) isopropoxide resulted in the formation of amorphous material and 3D zirconium silicate respectively. On the other hand, no matter of the Al source employed (metal Al, sodium aluminate and aluminium hydroxide) the system yielded feldspar.

Raman spectroscopy is a commonly used method to identify the presence of various structural features within zeolite (silicate) frameworks. It is especially convenient for detecting the small ring building units since three-membered rings exhibit bands in the region between 550 and 620 cm^{-1}, four-membered rings from 470 to 530 cm^{-1} and five-membered rings from 370 to

Table 1. Molar oxide composition of the starting reaction mixtures containing different T atoms and the phase composition of the product obtained at 180°C for different periods of time (t_c).

molar oxide composition of the starting reaction mixture	starting chemical	t_c (days)	final product
$1SiO_2$:0.1ZnO:0.5NaOH:0.5KOH:0.08TEAOH:$44H_2O$	ZnO	11	RUB-17
$1SiO_2$:0.05Al_2O_3:0.5NaOH:0.5KOH:0.08TEAOH:$44H_2O$	powder Al	12	feldspare type alumosilicates
$1SiO_2$:0.05Al_2O_3:0.5NaOH:0.5KOH:0.08TEAOH:$44H_2O$	$Al(OH)_3$	12	
$1SiO_2$:0.05Al_2O_3:0.5NaOH:0.5KOH:0.08TEAOH:$44H_2O$	$NaAlO_2$	12	
$1SiO_2$:0.05B_2O_3:0.5NaOH:0.5KOH:0.08TEAOH:$44H_2O$	B_2O_3	20	no precipitation
$1SiO_2$:0.05B_2O_3:0.5NaOH:0.5KOH:0.08TEAOH:$44H_2O$	$B(OH)_3$	12	boron phyllosilicate
$1SiO_2$:0.1GeO_2:0.5NaOH:0.5KOH:0.08TEAOH:$44H_2O$	GeO_2	12	mixture of germanium silicates
$1SiO_2$:0.1MgO:0.5NaOH:0.5KOH:0.08TEAOH:$44H_2O$	MgO	12	layered material
$1SiO_2$:0.1ZrO_2:0.5NaOH:0.5KOH:0.08TEAOH:$44H_2O$	$ZrOCl_2 \cdot 8H_2O$	25	amorphous
$1SiO_2$:0.1ZrO_2:0.5NaOH:0.5KOH:0.08TEAOH:$44H_2O$	Zr(IV) isopropoxide	20	3D zirconium silicate
$1SiO_2$:0.05Li_2O:0.5NaOH:0.5KOH:0.08TEAOH:$44H_2O$	$LiOH \cdot H_2O$	60	no precipitation
1.1SiO_2:0.5NaOH:0.5KOH:0.08TEAOH:$44H_2O$	TEOS	30	no precipitation

430 cm^{-1}. Bands in the range 290–410 cm^{-1} are attributed to six-membered rings while larger rings have bands below 290 cm^{-1}.[31,32] The Raman spectra of the solids prepared by employing various T atom sources are depicted in Figure S3. The three-membered rings characteristic for RSN-type material were not detected in the samples prepared in Al, B and Mg containing systems. Aluminium-containing products exhibit nearly identical spectra with main bands below 550 cm^{-1}. In the spectrum of $B(OH)_3$ synthesized product, there is a band with a maximum at 555 cm^{-1}, while MgO product has only one band at 683 cm^{-1}. The $ZrOCl_2 \cdot 8H_2O$ product spectrum does not have well defined bands in the frameworks rings region. There is a band at 602 cm^{-1} in the spectrum of GeO_2-containing system. This peak could be attributed to the 3MRs in the Ge product which is not a surprise considering a large number of germanium-containing zeolite materials with 3MRs in the structure.[18] Nevertheless, this system did not yield an RSN-type material. Furthermore, when Zr(IV) isopropoxide is employed, the end product features a band at 586 cm^{-1}. This kind of material comprises 3MRs as deduced on the grounds of the reported structural data.[29] However, in this silicate material, the zirconium has octahedral coordination and cannot be considered as zeolitic type material.

Clearly, under given conditions only zinc used as potential zeolite framework T atom together with silicon resulted in the formation of zeolitic three-membered ring containing RSN-type material. Thus, our attempt to replace the Zn in the RSN –type structure was not successful, which reveals its important structure-directing effect. In the following sections, we will present the results of the detailed study of the impact of the starting Zn compound on the properties of RUB-17 precursors and the final product.

Effect of zinc source

The XRD patterns of the solids obatiend with various zinc sources are depicted in Figure 1A. The peak positions in all of the patterns coincide with RSN framework type material. TG and dTG curves of selected solids all match well with the reference RUB-17[17] meaning that the composition of the final product and the water content in the samples are nearly identical (Figure S4). Furthermore, the Si/Zn ratios of the materials (Table S1) vary around the expected value of 3.5 in accordance with the particular site that zinc occupies in the RSN-type framework. The corresponding Raman spectra plotted in Figure 1B also correlate well with the reference RUB-17 material prepared from ZnO.[17] The spikes in the spectra of the solids prepared from ZnO and ZIF-8 are measurement artifacts. In each Raman spectrum of RUB-17, synthesized from various Zn sources, all four types of small rings present in the RSN framework are easily distinguished – 3MRs, 4MRs, 5MRs and 6MRs at 609, 507, 437 and 339 cm^{-1}, respectively. ^{29}Si MAS NMR spectra (Figure 1C) of the final products are identical. As found previously, there is an isolated peak at -82 ppm assigned to the Si atom surrounded by two Si atoms and two Zn atoms.[33] In RSN-type framework, such an environment can only be attained in the spiro position of the *lov*-unit. XRD, Raman and ^{29}Si MAS NMR data indicate the formation of solely RSN-type material in all of the studied systems after 11 days of hydrothermal treatment regardless of the employed Zn source.

In the studied reaction systems, the solid and liquid phases are visibly separated as the solid is precipitated at the bottom of the autoclave. Moreover, the solids are highly aggregated forming a hard monolith. The SEM micrographs of selected representative samples reveal different crystal size and morphology depending on the starting Zn chemical (Figure S5). In the samples

synthesised from ZnO and $ZnCl_2$ the crystals have a wide size distribution ranging between 100 and 1500 nm. Nearly all of the crystals grow together building up complex aggregates of different sizes. In ZnO and $ZnCl_2$ systems, the crystal faces are well-defined, and the edges are sharp. Their morphology is prismatic, ranging from short to long prisms. The crystals in ZIF-8 containing system differ significantly. There are two types of crystals – very small (~130 nm) with rounded edges and larger (~800 nm) having sharper edges and more pronounced crystal faces. These results suggest there is a difference in the crystal growth processes in the studied series of reaction systems.

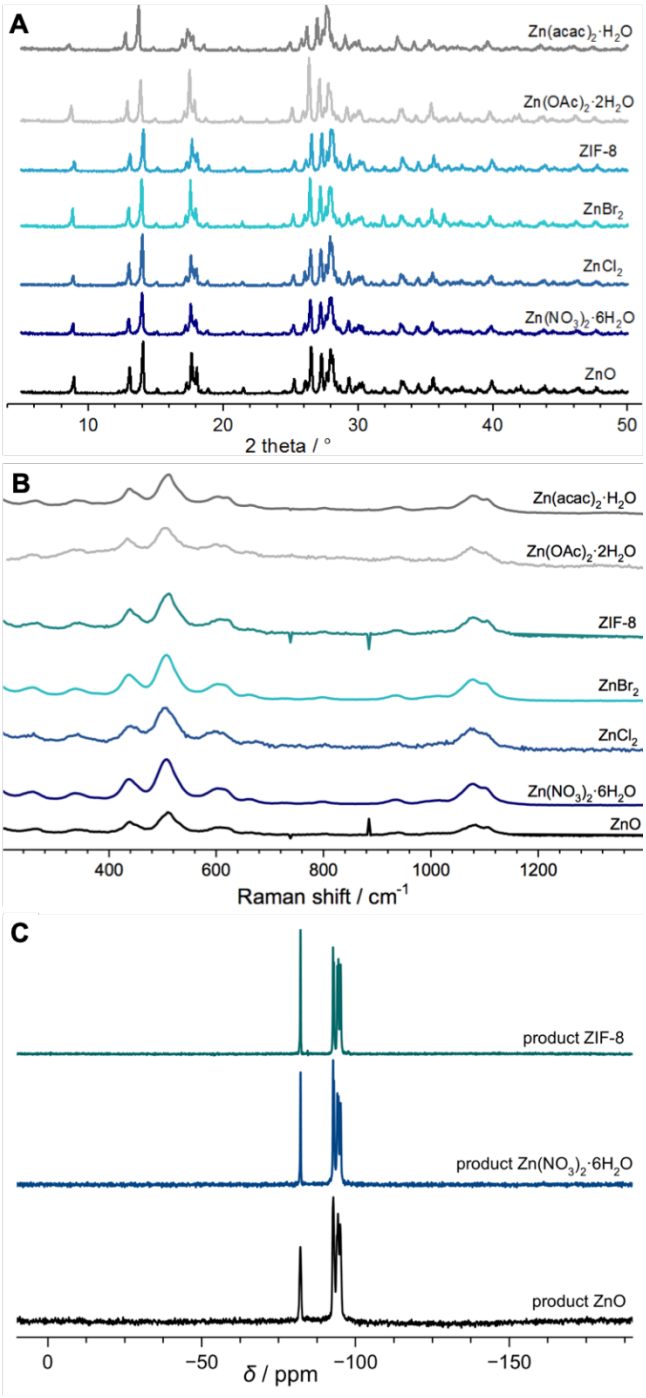

Figure 1. XRD patterns (A), Raman spectra (B) and NMR spectra (C) of the final products obtained after 11 days of hydrothermal treatment using different Zn sources.

Study of the precursors/reaction intermediates

XRD study

A previous study employing ZnO as initial zinc source has shown that the *lov*-units are formed in the very early stage of the RUB-17 crystallization – they were detected after only 8 h while the reaction was completed after 222 h.[17] Therefore, we started our study with the intermediates taken after 8 h of hydrothermal treatment. Powder XRD patterns of the 8 h precursors are displayed in Figure 2. Two different groups of samples can be observed. The samples from ZnO, $Zn(NO_3)_2 \cdot 6H_2O$, $ZnCl_2$ and $ZnBr_2$ (soluble salts) systems which comprise amorphous phase and zinc oxide while the samples from $Zn(OAc)_2 \cdot 2H_2O$, $Zn(acac)_2 \cdot H_2O$ and ZIF-8 (complex compounds) encompass solely amorphous phase. In the first set of samples, the zinc oxide is precipitated immediately upon the addition of base into the solution. On the other hand, based on the absence of any reflex in the X-ray pattern it can be concluded that the zinc acetylacetonate, ZIF-8 and zinc acetate are dissolved after 8 h at 180 °C. Furthermore, there is no precipitation of zinc oxide which suggests that in these systems Zn could be incorporated in the amorphous solid phase immediately upon the decomposition of the complex compounds, retained in the liquid phase bounded by ligands or present in some amount in both, the liquid and the solid phase.

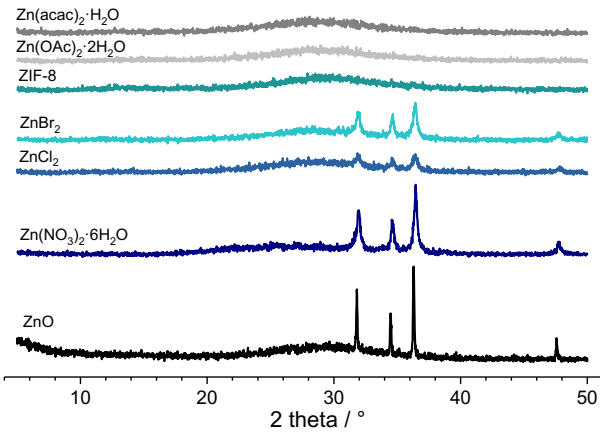

Figure 2. Powder XRD patterns of the reaction intermediate taken after 8 h of hydrothermal treatment of reaction mixtures prepared from various Zn sources at 180 °C.

The chemical analysis of the solid phases was performed by XRF in order to provide information on zinc distribution in the precursors. The molar Si/Zn ratios of the precursors taken after 8 h of the hydrothermal treatment (Table 2) indicate higher content of Zn in the solid phases of the systems prepared with ZIF-8, $Zn(OAc)_2 \cdot 2H_2O$ and $Zn(acac)_2 \cdot H_2O$ than in the water-soluble Zn salts. This result points out that the Zn from these compounds reacts immediately with the silica species . The precursor in which ZnO was used has a higher amount of Zn as well. In this case ZnO is directly added to the reaction mixture, not precipitated from the solution of Zn salts so less ZnO was dissolved. In the systems containing water soluble zinc salts ($Zn(NO_3)_2 \cdot 6H_2O$, $ZnCl_2$ and $ZnBr_2$) there is less Zn in the solid phase in spite of ZnO precipitation. Nevertheless, the yield of the solid phase recovered after 8 h and at the end of the crystallization (Table 2) has a reciprocal trend. The soluble zinc salts yield about 5 wt% of the

Table 2. Results on the chemical analysis of the studied precursors (column Si/Zn^{XRF} – 8 h), solid phase yields after 8 hours and 11 days, weight loss in the TG curves of the precursors and the positions of the dTG curve minumums (columns TG release – 8 h and dTG minimum – 8 h) and the GISAXS analysis (columns *R* and σ_R).

Starting chemical	Si/Zn^{XRF} – 8 h	solid phase yield – 8 h (wt%)	solid phase yield – 11 d (wt%)	TG release – 8 h (wt%)	dTG minimum – 8 h (°C)	*R* (Å)	σ_R (Å)
ZnO	2.01	2.07	2.31	-14.6	92.4; 117.3	10.2	12.5 (2.85)
$Zn(NO_3)_2 \cdot 6H_2O$	4.49	4.92	4.83	-13.5	96.8; 119.6	15.6	4.1 (7.7)
$ZnCl_2$	4.31	5.12	5.55	-13.9	97.3; 121.5	8.9	1.53 (7.2)
$ZnBr_2$	3.99	5.00	4.45	-13.2	96.3; 121.6	11.6	2.6 (7.01)
ZIF-8	3.11	2.95	2.87	-12.5	-; 117.0	20.5	8.65 (6.98)
$Zn(OAc)_2 \cdot 2H_2O$	2.63	2.69	2.58	-12.8	95.0; 116.7	17.6	9.85 (5.6)
$Zn(acac)_2 \cdot H_2O$	2.76	2.90	2.91	-12.1	96.1; 120.3	11.6	2.7 (7.05)

solid phase while ZnO and complex compounds result in an almost half lower quantity of the obtained material. Clearly, in the studied systems the precipitation of the solid phase is affected by the nature, concentration, and distribution of zinc species in the liquid phase. On the grounds of these data, it can be concluded that Zn bounded with organic ligands is more prone to react with Si species. Furthermore, in the complex compound systems, the solubility of zincolilicate species is higher. Finally, it can be conveyed that, similarly as Al, Ge, Zr and Mg, under the studied reaction conditions, Zn promotes the solid phase precipitation and that the final solid phase yield is low in all systems because of the high alkalinity of the system. The fact that no precipitate has been formed in the all silica system corroborates this reasoning.

Spectroscopic study

Raman spectra of the precursors taken after 8 h differ significantly from the spectrum of the fully crystalline RUB-17 (Figure 3). They are in accordance with the XRD findings that the $ZnBr_2$, $ZnCl_2$ and $Zn(NO_3)_2 \cdot 6H_2O$ 8 h precursors contain ZnO. The 3MRs have been clearly observed in the $Zn(acac)_2 \cdot H_2O$, ZnO, and ZIF-8 precursors. The peak corresponding to three-membered rings was not found in the other samples, most probably due to the low intensity of

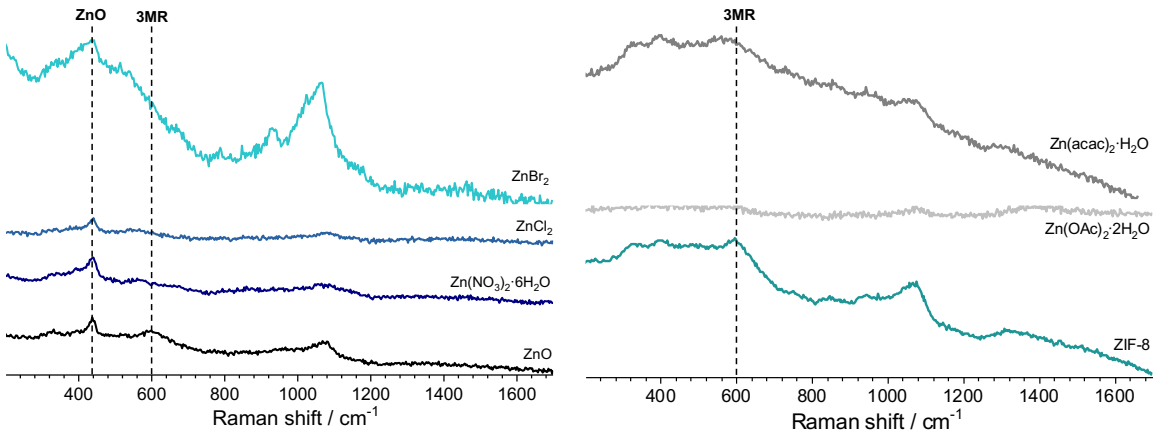

Figure 3. Raman spectra of the 8 h hydrothermally treated solids prepared by employing different Zn sources.

the signal. Peaks corresponding to other building units (4MRs, 5MRs and 6MRs) were not observed at this stage of the reaction. Hence, this finding represents a strong indication that in this kind of systems the 3MRs are the first zeolite framework building units to be formed.
According to the ^{29}Si {^{1}H} CP NMR spectra of the 8 h precursors depicted in Figure 4 there is a distribution of Si species in the solid phase of the samples. Different zinc sources exhibit an impact on the Si species distribution since the shape of the curves is a function of relative contributions of different species. The spectra range from -69 to -118 ppm which indicates that in all of the samples taken in the initial stage of the reaction there is a certain amount of Si which is located in the spiro position of the *lov*-unit. Namely, taking into account that the 3MRs have been detected in the Raman spectra of some of the samples and that in completely crystalline material the Si at spiro position exhibits a peak at -82 ppm it can be deduced that the three-membered rings connected to build the *lov*-units contribute to the NMR spectra of the 8 h precursors in the region around -80 ppm.

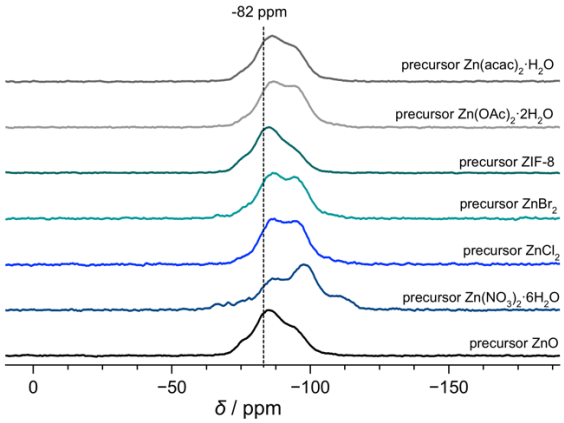

Figure 4. Normalized ^{29}Si {^{1}H} cross-polarization NMR spectra of the samples taken after 8 h of hydrothermal treatment of the reaction mixtures prepared by employing different Zn sources.

Figure S6 displays the FTIR spectra of the studied RUB-17 precursors and the crystalline RUB-17. The bands from 1300 to 760 cm^{-1} region are generally assigned to the asymmetrical O–T–O stretching mode, the symmetrical O–T–O stretching mode and the T–O bending mode of the TO_4 tetrahedra.[34] The peak positions in the spectra of the precursors coincide with the fully crystalline RUB-17 in this region. However, these peaks are less sharp in the spectra of the precursors. Furthermore, the peaks are shifted towards higher wavenumbers with respect to RUB-17. Clearly, the types of internal tetrahedra T–O chemical bonds are identical in both, the crystalline material and its precursors. Still, a significant degree of disorder is present in the precursor materials. Additional structural information (external tetrahedral linkage vibrations) can be obtained from the bands in the region below 750 cm^{-1} in the infrared spectra. The bands around 550 cm^{-1} is attributed to five membered rings in the structure.[34] RUB-17 does exhibit a weak band at 557 cm^{-1}. Moreover, there are three well resolved bands at 520, 445 and 408 cm^{-1}. Any of these bands are present in the spectra of the precursors suggesting once again there are no well-defined five membered rings, i.e. the parts of the RSN structure larger than *lov*-unit have not yet been formed. However, in this region the precursors exhibit broad noisy band

ranging from 540 to 400 cm^{-1} which indicates there are intertetrahedral bonds similar to the ones in the crystalline RUB-17 material.

UV/Vis spectral curves of the solid 8 h precursors (Figure 5) have the same trend as the commercial zinc oxide used as a starting compound in the ZnO-containing system. Likewise, they all exhibit a maximum at 365 nm and have an absorption edge value at 390 nm. However, the intensities of the spectra are significantly lower than the pure commercial ZnO. Besides, the spectra of the precursors differ substantially from the spectra of the starting Zn compounds both in curve shape and intensity (Figure S7). RSN-framework materials prepared in this study have an absorption edge position at 390 nm similar to both the precursors and zinc oxide. Although the bands in the spectra of the end products appear in the same wavelength range, there is a difference in their intensity which has been attributed to measurement execution conditions. The ZnO end product exhibits solid state UV/Vis curve oriented into the opposite direction than the precursor materials with the maximum positioned at 250 nm. This set of data suggest that the coordination of Zn differs in crystalline RUB-17 from the Zn coordination in the 8 h precursors. The surroundings of Zn in the precursors are more similar to the zinc oxide material than RUB-17. Further, this represents a strong indication that zinc undergoes three states of coordination during RUB-17 synthesis: 1) the coordination in the starting compound; 2) ZnO-like coordination; 3) coordination in RSN-type framework. It seems that the second coordination is essential for the formation of RUB-17 since it has been detected in all systems. In addition, the infrared and UV/VIS spectroscopy findings suggest that indeed there are similar chemical bonds (building units) in all of the studied 8 h precursors thus substantiating the conclusion there are *lov*-units present in these samples.

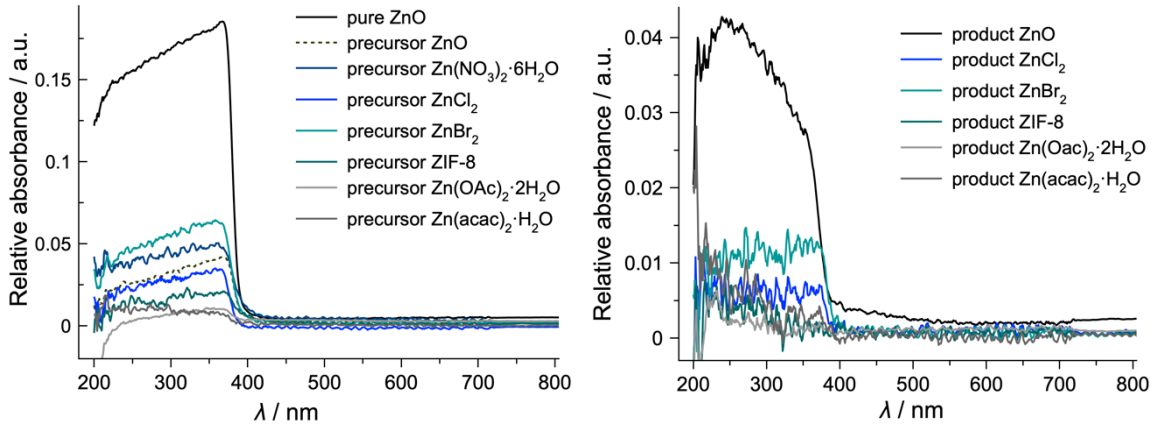

Figure 5. Solid state UV/Vis spectra of the precursors taken after 8 h hydrothermal treatment of the reaction mixtures with different Zn sources (left) and of the RUB-17 material obtained from different Zn sources (right).

Thermogravimetric analysis

TG curves of the solid phases taken after 8 h of hydrothermal treatment are plotted in Figure S8. They follow the same trend, but the total weight loss differs from one sample to another (column TG release – 8 h (wt%), Table 2). Although the differences are small, the general trend shows higher weight loss in soluble salt precursors which is due to more water present in the samples. Considering higher water content in precursors comprising precipitated ZnO which have higher Si content and yield higher quantity of the solid phase, it can be concluded that

indeed there are more silanol groups in precursors prepared from $ZnBr_2$, $ZnCl_2$ and $Zn(NO_3)_2 \cdot 6H_2O$. Obviously, the solid phase formed by the coprecipitation of Zn coming from dissolved complex compounds and Si species has lower affinity towards water due to exceeding amount of Zn-O-Si chemical bonds. In a fully crystalline RUB-17 material the quantity of water is lower since there are fewer silanol bonds in the crystalline material.[17] In the lower temperature regions, the dTG curves exhibit a similar shape. Indeed, it is typical for zeolites and zeolite-like materials to release the water below 200 °C and the position of the dTG minimum provides information on the strength of the water bonding.[16] In the studied set of samples the minimums are found at very similar temperatures (Table 2), which indicates that the water in all samples is bonded with approximately the same strength and consequently that there are similarties in the structure of the solids. This supports the spectroscopic data which shows the presence of nearly identical types of chemical bonds in all the precursors.

TEM microscopy

In order to obtain more insights in the local structure of RSN precursors, a TEM study of the 8 h precursors recovered from the ZnO and $Zn(NO_3)_2 \cdot 6H_2O$ reaction mixtures was performed (Figure 6). The gel particles exhibit a porous structure with the spherical voids distributed throughout the particles. The pore size is not uniform, and the dimensions vary from very small to rather large voids. Furthermore, there is a difference between the size of the voids in the two samples. Porous precursor gel particles have been found in many aluminosilicate zeolite yielding systems containing high concentrations of alkali cations.[35-37] The appearance and development of voids has been identified as an essential stage of the nucleation process and consequently crucial for the zeolite formation. As far as we know, this is the first report on the observation of voids within gel particles in zincosilicate precursors yielding a zeolite-type material.

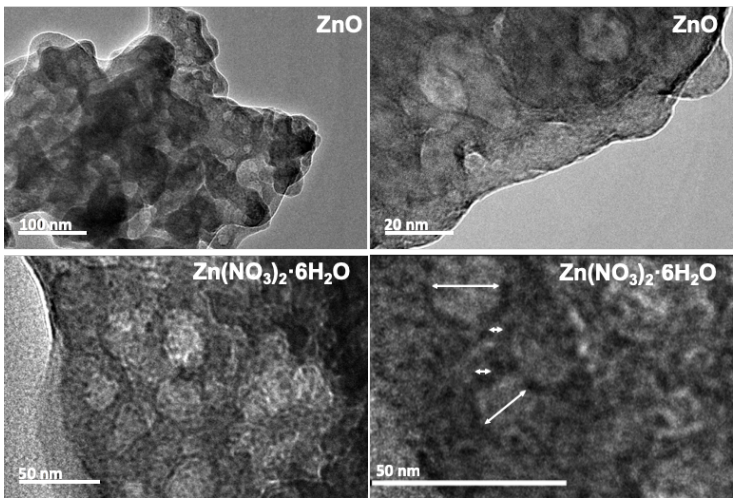

Figure 6. TEM images of the 8 h precursor samples prepared using different Zn sources. Arrows denote the dimensions of the voids.

GISAXS study

GISAXS was employed to get a deeper insight into the voids present in the samples. The amorphous precursors exhibit very low micropore (and mesopore) volumes compared to the

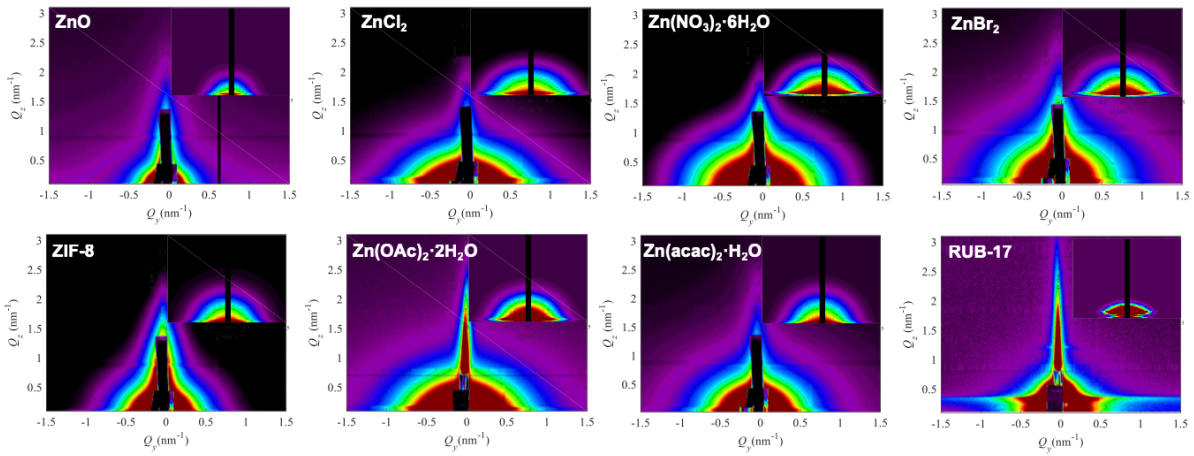

Figure 7. Grazing incidence small-angle X-ray scattering (GISAXS) patterns of the studied precursors and crystalline RUB-17 material. Insets represent simulated patterns obtained using the parameters obtained by the fit.

fully crystalline zeolite.[38-40] Melinte et al. performed a very detail analysis of gel particles containing such voids and found that they contain shell which is impermeable for N_2.[35] The majority of the mesopores exhibit diameter between 3 and 20 nm, more than 40% of the pores having a diameter between 5 and 7 nm. Consequently, any gas adsorption method could provide reliable information on the inherent porosity of the zeolite precursor samples due to the nonporous zone covering gel particles. Therefore, we employed GISAXS analysis, which provides naoscale information on the structure on the structure of the material. GISAXS maps obtained on the studied samples are displayed in Figure 7. All maps show semi-circular intensity distribution with different characteristic radius. The maps show no correlation peaks that could be related to the presence of ordered nanostructures in the materials, so a simple model including a spherical shape of the nanovoids was used to fit the experimental data. Such approximation is supported by the TEM findings. The parameters of the fit were the radius of the voids (R) and the size distribution parameter σ_R representing the standard deviation of the distribution. The gamma distribution of the void sizes was used for the fit. The measured GISAXS range ($Q_{y,z} \sim 0$ to 3 nm^{-1}) is suitable for the analysis of void sizes of a few nanometres. The GISAXS signal of larger voids appears at small Q values where is superimposed to the surface roughness contribution, which is not taken into account in the present GISAXS analysis. Therefore, the measurement is more sensitive to smaller structures that are visible in the TEM images (Figure 6), not to the large ones (R>10 nm). The parameters obtained by fit to describe the collected GISAXS patterns are listed in Table 2, columns R and σ_R. In the precursor samples, the radii are ranging from 8.9 Å to 21 Å. This diameter ranging from 2 to 4 nm is comparable with the dimensions of the smallest pores observed in TEM images as well as with the void size observed in EMT-type alumosilicate zeolite precursor.[35] Voids with similar size were detected even in the completely crystalline RUB-17. These voids most probably origiante from the texture of the agglomerated crystals.

In addition, the applied model enabled calculating the pore size distribution for each sample (Figure 8). The data indicate that the distribution curves differ depending on the employed zinc source. Clearly, the overall chemical composition of the reaction mixture determines the structure of the gel particles.

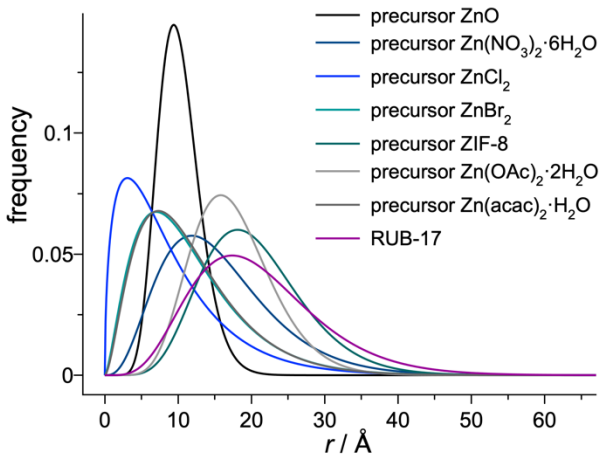

Figure 8. Calculated spherical voids radii distribution curves for the 8 h precursors prepared using various zinc sources.

DFT modelling of the formation of *lov*-unit

The formation of the *lov*-unit is a complex process and therefore different possibilities have to be considered. The formation of the T–O–T bridges is the two-step process, with the first being the formation of the T–O bond leading to the 5-coordinated T site, and the other being a water release.[41] Depending on the type of the oligomer and its composition, either of the steps can be a limiting one in the reaction. It has to be underlined that for the pure silica system the final configuration was still a 5-coordinated Si atom, and the bond cleavage was observed. That means the thermodynamics of this process could not be correctly evaluated; however as the product of two pathways was always the same - the thermodynamics does not play a role in the determination of the mechanism.

Two options have been considered for the formation of the *lov*-unit by the direct ring closure - one route (route 1) depends on the fully formed *ste* unit (defined by the IZA Structure Commission),[18] and assumes the oxygen bridge is already formed between two Si sites in the *ste* unit, and ring closure yields the *lov*-unit. The other route (route 2) assumes the opposite - the *lov*-unit is already formed, and upon the reaction, it gets embedded to the surface yielding *ste*-unit. For sake of comparison, the pure silica system, with Si atom in place of the heteroatom has also been considered and will be discussed first.

The energy profile of the reaction with the 5-coordinated Si atom at the *ste* (route 2) with the water molecule attached is not shown, yet the formation of this state leads via the negligible barrier of 10 kJ/mol, and the subsequent step of water release is spontaneous and stabilize the system by 68 kJ/mol with respect to the 5-coordinated intermediate. Note that this intermediate is additionally stabilized by the hydrogen bond between the water and the oxygen of the top Si atom. The final product, the 3MR, is thermodynamically stable. Expectedly, it is similar to the route 1 pathway, because both these systems contain 5-coordinated Si atom, thus are chemically similar and differ only in the constraints. This result leads to the conclusion that once the *ste* unit is formed, the ring closure is a relatively easy and feasible process.

The situation is very similar for Al system, however for pathway 1, the reaction is thermoneutral. There is no significant thermodynamic driving force, and additionally, the kinetic barrier is relatively high, compared to other investigated systems (87 kJ/mol). This allows us to conclude that the formation of the *lov*-unit with the Al atom is unlikely. On the

other hand, the formation of the *ste* unit with Al heteroatom should be considered an easy process. The process is exothermic by 57 kJ/mol and is accompanied by the barrier of only 47 kJ/mol. The only problem in this process is that it assumes the *lov*-unit is already formed in a reaction similar to pathway 1, which is much more difficult. The formation of the 3-membered ring with the Al atom in one T-site is thus the limiting step of the process of Al-containing RSN-type material formation.

The system containing zinc behaves similarly in both investigated pathways as shown in Figure S9, and contrary to all other systems reaction occurs in one concerted step (indeed, the water release in Si and Al systems is very easy, but still it is activated process). Both pathways are only slightly exothermic (approximately 25 kJ/mol) with a low activation barrier of 40 kJ/mol. In addition, contrary to the Al and Si systems, the 5-coordinated Zn atom has not been observed, and rather the Zn–O bond cleavage occurs easier, leading to the Zn in the planar geometry.

All results suggest that the Zn significantly facilitates the formation of 3MRs. However both routes - either the embedding the 3MR into the growing crystal and 3MR closure at the surface - are equally probable. On the other hand - the small barriers suggest the preparation process should occur much faster than observed experimentally. This suggests that there is another rate limiting step during the synthesis.

Discussion

There is a large interest to prepare RSN-type zeolite materials due to the presence of nine-membered rings which offer new possibilities in zeolite application. So far, the only representative material having this framework is zincosilicate RUB-17. In the current investigation we have attempted to introduce several possible T-atoms (Al, Ge, B, Mg, Li, Zr) in the framework of RSN-type zeolite material by employing the identical reaction conditions as for the preparation of zincosilicate RUB-17. These elements were selected because they can build three-membered rings in silicate systems and because the three-membered rings were found in most zeolite structures comprising odd-numbered pores. Yet, RSN-type or any other zeolite-type material have not been prepared under studied conditions when before-mentioned T atoms were employed. Moreover, the reaction mixture comprising solely Si did not yield any solid precipitate, let alone zeolite-type material. On the other hand, no matter which zinc initial chemical was used, RSN-type zeolite material was always produced indicating the vital role of zinc in the formation of this material. On that account, the 8 h precursors have been isolated and subjected to thorough characterization to provide more data on RSN-type material forming. There is a difference between the 8 h precursors prepared from the soluble zinc salts and complex zinc compounds in terms of their phase composition as revealed by XRD and Raman spectroscopy. Namely, zinc oxide precipitates upon the addition of hydroxide into zinc salts solutions, while in the complex compounds systems zinc is coordinated with different ligands which prevent ZnO precipitation. This further reflectes in the chemical composition of the solid and liquid phase as well as in the solid phase yield. When ZnO is formed, the silicate precipitation is favoured and consequently the Si/Zn ratio and the quantity of the solid phase are higher. Using complex zinc compounds leads to precipitation of less material of higher zinc content. As the reaction advances, the Si/Zn ratio of the solid changes until the final value of 3.5 in the crystalline material. However, the amount of the materials recovered at the end of the reaction is very similar to that in the 8 h samples. These data suggest that in the preparation of

RUB-17 the properties of Zn source and the equilibrium between the Zn species in the liquid phase and solid phase play an important role in the overall reaction mechanism. It can be assumed that both Zn species from both solid and liquid phase react with Si species to form RUB-17, but it seems that the liquid phase mediated processes are the dominating ones.

Based on the spectroscopic measurements (NMR, IR, Raman, UV/Vis) and TG analysis it can be deduced that there are similar chemical bonds in the studied series of samples, yet the distribution of the present species is different. The results suggest there are three-membered rings connected to form *lov*-unit in all 8 h precursor samples. These data indicate that although *lov*-units are formed during the initial phase of the zeolite formation (8 h), the subsequent processes of establishing long range order and assuming needed Zn coordination are rather complex and consequently it takes a longer time for the formation of entirely crystalline material (11 d)[17]. A possible explanation could be an early, yet rapid precipitation of the solid phase which has a limited surface area exposed to the liquid phase. Namely, after 8 h of hydrothermal treatment at 180 °C the solid yield is quite low (less than 6 wt% in all of the systems – Table 2) and there are already basic building units present but the reaction is still long. Obviously the frequency of successful chemical reactions in terms of RSN-type framework building is low once the solid phase gets precipitated. This once again leads to the conclusion that in the studied system the solution mediated processes prevail over solid phase rearrangement.

TEM images of the selected samples revealed the presence of spherical voids within the precursor particles. The voids were further probed by GISAXS. Despite not being quantitative, the pore size distribution varies with the employed zinc source thus showing that the chemical composition of the reaction mixture directly affects the gel structure. Core-shell structure of zeolite precursor particles with porous core was observed in aluminosilicate synthesis systems with a high concentration of alkali cations.[35] It was concluded that the mother liquor is entrapped inside the pores due to the impermeable shell and that the onset of zeolite nucleation takes place at the shell part. Consequently, the external surface of the initial gel particles governs the entire crystallization process. If this reasoning is applied to the zincosilicate system studied herein, it can explain the formation of highly intergrown crystals in the end product. Taking into consideration that the reaction is completed after a long period of time, in spite of the structure building units formed in the early stage of the reaction, the external surface area of the precursor particles exposed to the liquid phase should be low or the number of RSN-type nuclei able to grow is small. Finally, the zincosilicate zeolite precursors have a structure similar to aluminosilicate zeolite precursors and obviously the events taking place at the molecular level direct the final product.

The experimental findings in this work are corroborated with the theoretical investigations. Namely, the results of the DFT modelling suggest that the limiting step in the system where Al would be located in one of the T sites is the three-membered ring formation. On the other hand, Zn strongly favours the 3MRs formation regardless of the process pathway. Moreover, the low barrier energy values indicate that the overall RUB-17 crystallization should take place more rapidly than it, in fact, does which once again leads to the conclusion that there is some still unknown process which determines the RUB-17 formation. Since a variety of zinc sources has been studied herein in terms of the zinc state and chemical bonds, it can be deduced that the observed effect does not arise due to the differences in the availability of Zn neither various

anions present in the system. Nevertheless, considering that there are *lov*-units in the initial stage of the reaction, yet Zn has ZnO-like coordination, it can be argued that the Zn coordination change is the limiting step here. However, the finding of the exact reason will be pursued in further studies.

Conclusion

Set of complementary experimental techniques employed in this study provided new insights into the formation of RSN-type material. We were able to prepare RSN-type material exclusively from Zn containing systems under the studied reaction conditions. Moreover, seven different Zn chemicals having different nature of chemical bonds were used and RUB-17 was obtained in each reaction system. For comparison, in the "classical" alumosilicate zeolite synthesis systems the end product and its properties are substantially determined by the T atom source, particularly silicon source.[42,43] Obviously, the ability of zinc to bind silicon in this specific way is so strong that the reaction takes place no matter the stability and solubility of the starting Zn compound. The collected results, both experimental and theoretical, indicate the Zn notably facilitates the formation of the three-membered rings which are formed in the very early stage of the reaction. Conversely, the whole reaction is rather long suggesting there are some other processes which impact the RUB-17 crystallization. Indeed, it appears that in this case there is a genuine structure directing effect of zinc atoms.

Acknowledgements

The financial support from the Croatian Academy of Science is gratefully acknowledged. M.B. thanks Croatian Science Foundation, project number O-2594-2018. B.Sz. would like to acknowledge the support from Polish Minsitry of Science and Higher Education for statutory subsidy activity for Faculty of Chemistry at Wrocław University of Science and Technology for the year 2019. D.M. and M.Č. were supported by University of Rijeka under the project number 13.2.1.3.04. The authors would like to thank dr. Željka Petrović for collecting SEM images.

References

1 J. B. Nagy, P. Bodart, I. Hannus and I. Kiricsi, *Synthesis and use of zeolitic microporous materials*; DecaGen: Szeged-Szõreg, 1998.

2 C. J. Rhodes, *Annu. Rep. Prog. Chem., Sect. C*, 2007, **103**, 287-325.

3 M. Reháková, S. Čuvanová, M. Dzivák, J. Rimár, and Z. Gaval'ová, *Curr. Opin. Solid State Mater. Sci.*, 2004**, 8**, 397-404.

4 J. Perić, M. Trgo, N. Medvidović Vukojević and I. Nuić, *Separ. Sci. Technol.*, 2009, **44**, 3113-3127.

5 A. Dyer, *Introduction to Zeolite Science and Practice – 3rd Revised Edition*, J. Čejka, H. van Bekkum, A. Corma and F. Schüth (Eds), Elsevier, 2007, 525-553.

6 B. Bogdanov, D. Georgiev, K. Angelova and Y. Hristov, *Proceedings of the International Scientific Conference "Economics and Society development on the Base of Knowledge"*; S. Atanasova, G. Kostov, V. Mileva and T. Ivanova (Eds.), Union of Scientists – Stara Zagora: Stara Zagora, 2009, Vol. 4, 1-5.

7 P. A. Wright, and M. Lozinska, *Zeolites and Ordered Porous Solids: Fundamentals and Applications*; C. Martínez and J. Pérez-Pariente (Eds.), Editorial Universitat Politècnica de València: Valencia, 2011, 1-36.
8 W. Vermeiren and J.-P. Gilson, *Top. Catal.*, 2009, **52**, 1131-1161.
9 A. Vasile and A. M. Busuioc-Tomoiaga, *Mater. Res. Bull.*, 2012, **47**, 35-41.
10 R. Bai, Q. Sun, N. Wang, Y. Zou, G. Guo, S. Iborra, A. Corma and J. Yu, *Chem. Mater.*, 2016, **28**, 6455-6458.
11 P. Chlubná, W. J. Roth, H. F. Greer, W. Zhou, O. Shvets, A. Zukal, J. Čejka and R. E. Morris, *Chem. Mater.*, 2013, **25**, 542-547.
12 V. Valtchev, E. Balanzat, V. Mavrodinova, I. Diaz, J. El Fallah and J.-M. Goupil, *J. Am. Chem. Soc.*, 2011, **133**, 18950-18956.
13 R. Martínez-Franco, C. Paris, M. E. Martínez-Armero, C. Martínez, M. Moliner and A. Corma, *Chem. Sci.*, 2016, **7**, 102-108.
14 D. P. Serrano, J. M. Escola and P. Pizarro, *Chem. Soc. Rev.*, 2013, **42**, 4004-4035.
15 Z. Qin, J.-P. Gilson and V. Valtchev, *Curr. Opin. Chem. Eng.*, 2015, **8**, 1-6.
16 A. Palčić, B. Subotić, V. Valtchev and J. Bronić, *CrystEngComm*, 2013, **15**, 5784-5791.
17 A. Palčić, F. Zapata Abellán, A. Vicente, C. Fernandez, V. Georgieva, J. Bronić and V. Valtchev, *CrystEngComm*, 2015, **17**, 7063-7069.
18 http://www.iza-online.org (accessed 17.4.2019.)
19 J. A. Walmsley and F. Walmsley, *Chemical Principles, Properties, and Reactions in the Laboratory*, Addison-Wesley: Reading, MA, 1985, 180-182.
20 T. Friščić, I. Halasz, P. J. Beldon, A. M. Belenguer, F. Adams, S. A. J. Kimber, V. Honkimäki and R. E. Dinnebier, *Nat. Chem.*, 2013, **5**, 66-73.
21 P. Van Espen, K. Janssens and J. Nobels, *Chemom. Intell. Lab. Syst.*, 1986, **1**, 109-114.
22 http://homer.zpr.fer.hr/gisaxstudio/doku.php (accessed 17.4.2019.)
23 M. Buljan, N. Radić, S. Bernstorff, G. Dražić, I. Bogdanović-Radović and V. Holý, *Acta Cryst. A*, 2012, **68**, 124-138.
24 J. P. Perdew, K. Burke and M. Ernzerhof, *Phys. Rev. Lett.*, 1996, **77**, 3865-3868.
25 http://www.cp2k.org/ (accessed 17.4.2019.)
26 J. VandeVondele and J. Hutter, *J. Chem. Phys.*, 2007, **127**, 114105.
27 S. Nosé, *J. Chem. Phys.*, 1984, **81**, 511-519.
28 S. H. Park, P. Daniels and H. Gies, *Micropor. Mesopor. Mater.*, 2000, **37**, 129-143.
29 D. M. Poojary, A. I. Bortun, L. N. Bortun and A. Clearfield, *Inorg. Chem.*, 1997, **36**, 3072-3079.
30 S. Kohara, J. Akola, H. Morita, K. Suzuya, J. K. R. Weber, M. C. Wilding and C. J. Benmore *PNAS*, 2011, **108(36)**, 14780-14785.
31 P. K. Dutta, D. C. Shieh and M. Puri, *Zeolites*, 1988, **8**, 306-309.
32 Y. Yu, G. Xiong, C. Li, and F.-S. Xiao, *Micropor. Mesopor. Mater.*, 2001, **46**, 23-34.
33 M. A. Camblor, M. E. Davis, *J. Phys. Chem.*, 1994, **98**, 13151-13156.
34 C. Li and Z. Wu, *Handbook of Zeolite Science and Technology*; S. M. Auerbach, C. A. Carrado and P. K. Dutta (Eds.), Marcel Dekker: New York, 2003; 423-515.
35 G. Melinte, V. Georgieva, M.-A. Springuel-Huet, A. Nossov, O. Ersen, F. Guenneau, A. Gedeon, A. Palčić, K. N. Bozhilov, C. Pham-Huu, S. Qiu, S. Mintova and V. Valtchev, *Chem. Eur. J.*, 2015, **21**, 18316-18327.

36 V. Valtchev, S. Rigolet and K. N. Bozhilov, *Micropor. Mesopor. Mater.*, 2007, **101**, 73-82.
37 V. Valtchev and K. N. Bozhilov, *J. Am. Chem. Soc.*, 2005, **127**, 16171-16177.
38 S. Inagaki, K. Thomas, V. Ruaux, G. Clet, T. Wakihara, S. Shinoda, S. Okamura, Y. Kubota and V. Valtchev, *ACS Catal.*, 2014, **4**, 2333-2341.
39 L. Itani, K. N. Bozhilov, G. Clet, L. Delmotte and V. Valtchev, *Chem. Eur. J.*, 2011, **17**, 2199-2210.
40 D. P. Serrano, R. van Grieken, M. E. Davis, J. A. Melero, A. Garcia and G. Morales, *Chem. Eur. J.*, 2002, **8(22)**, 5153-5160.
41 T. T. Trinh, A. P. J. Jansen and R. A. van Santen, *J. Phys. Chem. B*, 2006, **110(46)**, 23099-23106.
42 T. Antonić Jelić, B. Subotić, V. Kaučič and R. W. Thompson, *Stud. Surf. Sci. Catal.*, 1999, **125**, 13-20.
43 M. L Occelli, S. Biz, A. Auroux and G. J. Ray, *Micropor. Mesopor. Mater.*, 1998, **26**, 193-213.